PSA-Stratified Performance of ^{18}F- and ^{68}Ga-PSMA PET in Patients with Biochemical Recurrence of Prostate Cancer

Felix Dietlein[1,2], Carsten Kobe[1,2], Stephan Neubauer[3], Matthias Schmidt[1,2], Simone Stockter[1], Thomas Fischer[1], Klaus Schomäcker[1], Axel Heidenreich[4], Boris D. Zlatopolskiy[5], Bernd Neumaier[5], Alexander Drzezga*[1,2], and Markus Dietlein*[1,2]

[1]Department of Nuclear Medicine, University Hospital of Cologne, Cologne, Germany; [2]Center of Integrated Oncology Cologne Bonn, University Hospital of Cologne, Cologne, Germany; [3]West-German Prostate Center, Klinik am Ring, Cologne, Germany; [4]Department of Urology, University Hospital of Cologne, Cologne, Germany; and [5]Institute of Radiochemistry and Experimental Molecular Imaging, University Hospital of Cologne, Cologne, Germany

Several studies outlined the sensitivity of ^{68}Ga-labeled PET tracers against the prostate-specific membrane antigen (PSMA) for localization of relapsed prostate cancer in patients with renewed increase in the prostate-specific antigen (PSA), commonly referred to as biochemical recurrence. Labeling of PSMA tracers with ^{18}F offers numerous advantages, including improved image resolution, longer half-life, and increased production yields. The aim of this study was to assess the PSA-stratified performance of the ^{18}F-labeled PSMA tracer ^{18}F-DCFPyL and the ^{68}Ga-labeled reference ^{68}Ga-PSMA-HBED-CC. **Methods:** We examined 191 consecutive patients with biochemical recurrence according to standard acquisition protocols using ^{18}F-DCFPyL (n = 62, 269.8 MBq, PET scan at 120 min after injection) or ^{68}Ga-PSMA-HBED-CC (n = 129, 158.9 MBq, 60 min after injection). We determined PSA-stratified sensitivity rates for both tracers and corrected our calculations for Gleason scores using iterative matched-pair analyses. As an orthogonal validation, we directly compared tracer distribution patterns in a separate cohort of 25 patients, sequentially examined with both tracers. **Results:** After prostatectomy (n = 106), the sensitivity of both tracers was significantly associated with absolute PSA levels ($P = 4.3 \times 10^{-3}$). Sensitivity increased abruptly, when PSA values exceeded 0.5 μg/L ($P = 2.4 \times 10^{-5}$). For a PSA less than 3.5 μg/L, most relapses were diagnosed at a still limited stage ($P = 3.4 \times 10^{-6}$). For a PSA of 0.5–3.5 μg/L, PSA-stratified sensitivity was 88% (15/17) for ^{18}F-DCFPyL and 66% (23/35) for ^{68}Ga-PSMA-HBED-CC. This significant difference was preserved in the Gleason-matched-pair analysis. Outside of this range, sensitivity was comparably low (PSA $<$ 0.5 μg/L) or high (PSA $>$ 3.5 μg/L). After radiotherapy (n = 85), tracer sensitivity was largely PSA-independent. In the 25 patients examined with both tracers, distribution patterns of ^{18}F-DCFPyL and ^{68}Ga-PSMA-HBED-CC were strongly comparable ($P = 2.71 \times 10^{-8}$). However, in 36% of the PSMA-positive patients we detected additional lesions on the ^{18}F-DCFPyL scan ($P = 3.7 \times 10^{-2}$). **Conclusion:** Our data suggest that ^{18}F-DCFPyL is noninferior to ^{68}Ga-PSMA-HBED-CC, while offering the advantages of ^{18}F labeling. Our results indicate that imaging with ^{18}F-DCFPyL may even exhibit improved sensitivity in localizing relapsed tumors after prostatectomy for moderately increased PSA levels. Although the standard acquisition protocols, used for ^{18}F-DCFPyL and ^{68}Ga-PSMA-HBED-CC in this study, stipulate different activity doses and tracer uptake times after injection, our findings provide a promising rationale for validation of ^{18}F-DCFPyL in future prospective trials.

Key Words: PSMA ligands; prostate cancer; biochemical recurrence; ^{68}Ga-PSMA-HBED-CC; ^{18}F-DCFPyL

J Nucl Med 2017; 58:947–952
DOI: 10.2967/jnumed.116.185538

After radical prostatectomy, concentrations of prostate-specific antigen (PSA) typically decrease below detection threshold. A renewed increase in PSA levels to above 0.2 μg/L, commonly referred to as biochemical recurrence (BCR), signifies a potential relapse of prostate cancer after surgery (*1*). Similarly, BCR is defined as a PSA increase of at least 2 μg/L above the minimum PSA level after radiotherapy. The prostate-specific membrane antigen (PSMA) is particularly overexpressed on the surface of prostate cancer cells (*2*). Tracers for PET, that bind specifically to PSMA, have gained increasing attention for localization of tumors in BCR patients (*3–12*). In particular, ^{68}Ga-PSMA-HBED-CC displays substantial sensitivity in detecting tumor relapse after prostatectomy, even when PSA levels are low (≥0.2 μg/L) (*3–9*). Furthermore, 4 studies have consistently shown that approximately 95% of the ^{68}Ga-PSMA-HBED-CC–positive lesions have histologic tumor correlates in biopsies and surgical resections (*13–16*).

The short half-life of ^{68}Ga makes ^{68}Ga-PSMA-HBED-CC inconvenient for longer transport, so that cost-intensive, local gallium generators are required, which typically have lower yields at the end of their first half-life (*17*). Furthermore, the resolution of ^{68}Ga-labeled tracers is physically limited because of positron range effects (*18*). In contrast, ^{18}F labels avoid these intrinsic difficulties and can be produced at high yields in central cyclotrons. In 2011, the first preclinical data with the ^{18}F-labeled PSMA

Received Oct. 13, 2016; revision accepted Nov. 25, 2016.
For correspondence or reprints contact: Felix Dietlein, Department of Nuclear Medicine, University Hospital of Cologne, Kerpener Strasse 62, 50937 Cologne, Germany.
E-mail: felix.dietlein@uni-koeln.de
*Contributed equally to this work.
Published online Dec. 1, 2016.

ligand DCFPyL were published (*10*). Recently, 2 proof-of-principle studies demonstrated the general capability of ^{18}F-DCFPyL to detect relapsed tumors in 9 (*11*) and 14 BCR patients (*12*), respectively. Here, we examined 62 BCR patients with ^{18}F-DCFPyL and benchmarked the PSA-stratified sensitivity of ^{18}F-DCFPyL against ^{68}Ga-PSMA-HBED-CC (n = 129 patients).

MATERIALS AND METHODS

Patients

We examined 191 consecutive prostate cancer patients with BCR after radical prostatectomy (n = 106) or radiotherapy (n = 85), either with ^{18}F-DCFPyL (n = 62) or ^{68}Ga-PSMA-HBED-CC (n = 129) (Table 1). Patients were selected according to the following criteria: for the prostatectomy cohort—complete removal of the entire prostate gland (R0 or R1 resection) and a recent PSA increase to 0.2 μg/L or more after nadir; and for the radiotherapy cohort—organ-preserving local treatment (external-beam radiation therapy, brachytherapy, seed implantation, high-intensity focused ultrasound) and a PSA increase of at least 2.0 μg/L above the minimum PSA value after therapy, as determined by the referring urologist.

Additionally, we required that no distant metastases had been detected in previous examinations, that patients did not receive antiandrogen therapy, and a time period of at least 6 mo had elapsed between the initial therapy and the PET scan. Forty-seven of our prostatectomy patients received additional salvage radiotherapy before the PET scanning (16 ^{18}F-DCFPyL cases, 31 ^{68}Ga-PSMA-HBED-CC cases).

As an additional approach, we continued our efforts of a previous study (*12*) (n = 14 patients) and sequentially examined prostate cancer patients with ^{68}Ga-PSMA-HBED-CC and ^{18}F-DCFPyL. This allowed a direct comparison of the tracer distribution pattern within a separate validation cohort of 25 patients. Inclusion criteria for this validation cohort were described previously (*12*).

This study was conducted in accordance with the Institutional Review Board. All patients gave written informed consent to PET imaging and inclusion of their data in a retrospective analysis. All procedures were performed in compliance with the regulations of the responsible local authorities (District Administration of Cologne, Germany).

Imaging

PSMA PET tracers were synthesized as previously described for ^{18}F-DCFPyL (*10,12*) and ^{68}Ga-PSMA-HBED-CC (*19,20*). Each week, we produced 3 independent batches of ^{68}Ga-PSMA-HBED-CC and 1 batch of ^{18}F-DCFPyL. Patients were randomly assigned by tracer availability. Images were acquired on a Biograph mCT Flow (Siemens) PET/CT scanner. In accordance with standard acquisition protocols (*3,5,7,12*), patients fasted for at least 4 h before intravenous injection of ^{68}Ga-PSMA-HBED-CC (158.9 ± 45.1 MBq) or ^{18}F-DCFPyL (269.8 ± 81.8 MBq). PET images were acquired 1 or 2 h after injection, respectively. The same filters and acquisition times were used for both tracers. Non–contrast-enhanced (low-dose) CT scans were acquired in parallel to PET imaging. Images were reconstructed on the basis of the ultra-high definition algorithm (*21*).

PSMA PET scans were analyzed through visual inspection by at least 1 specialist in nuclear medicine and 1 specialist in radiology. A scan was scored as positive if focal tracer accumulation was detected in the prostate fossa, in a lymph node, or at a distant site. To be interpreted as a PET-positive lymph node, we required a morphologic correlate on the CT scan. A tumor relapse was interpreted as limited if tracer accumulation was limited to the prostate fossa or to locoregional lymph nodes. Otherwise, a positive scan was scored as advanced. Furthermore, we scored PET positivity based on the number of PET-positive lesions (score 0, negative scan; score 1, 1 lesion; score 2, 2 lesions; score 3, more than 2 positive lesions).

Confirmation of PET-Positive Lesions Through Biopsies

As an external validation of our imaging results, 15 BCR patients with PET-positive tissue within the prostate fossa underwent biopsy (4 ^{18}F-DCFPyL and 11 ^{68}Ga-PSMA-HBED-CC cases). For each patient, we obtained 12 local biopsies from the residual prostate gland (13 radiotherapy patients) or prostate fossa (2 prostatectomy patients), guided by ultrasound. We compared histology with tracer distribution and categorized the findings as follows: full concordance—all PSMA-positive segments histologically confirmed, all PSMA-negative

TABLE 1
Characteristics of Patients Examined in This Study

Characteristic	Prostatectomy		Radiotherapy	
	^{68}Ga	^{18}F	^{68}Ga	^{18}F
No. of patients	68	38	61	24
Age (y)	70.1 ± 7.9	68.4 ± 7.0	72.1 ± 6.7	71.8 ± 8.5
Weight (kg)	88.1 ± 16.2	87.9 ± 13.5	84.1 ± 12.5	90.5 ± 15.1
Height (cm)	179 ± 6.9	179 ± 7.1	178 ± 6.5	180 ± 5.6
Median time between therapy and PSMA PET imaging (mo)	61.2 ± 68.4	44.2 ± 49.7	55.3 ± 55.4	38.1 ± 38.3
PSA level (μg/L)	2.5 ± 2.2	2.7 ± 3.8	8.5 ± 11.1	4.1 ± 7.5
Initial TNM staging with T ≤ 2	58.3%	46.4%	100%	83.3%
Gleason score				
≤6	19.1%	11.2%	46.9%	0%
7	48.9%	48.1%	37.5%	68.8%
≥8	32.0%	40.7%	15.6%	31.2%

Patients were subdivided according to previous therapy (prostatectomy vs. radiotherapy) and tracer applied (^{68}Ga: ^{68}Ga-PSMA-HBED-CC vs. ^{18}F: ^{18}F-DCFPyL). On the basis of Gleason scores, patients were subdivided into moderately differentiated (≤6), moderately to poorly differentiated (=7), and poorly differentiated cases (≥8). Additionally, a fraction of patients initially displaying limited local tumor infiltration (TNM classification, T ≤ 2) is shown.

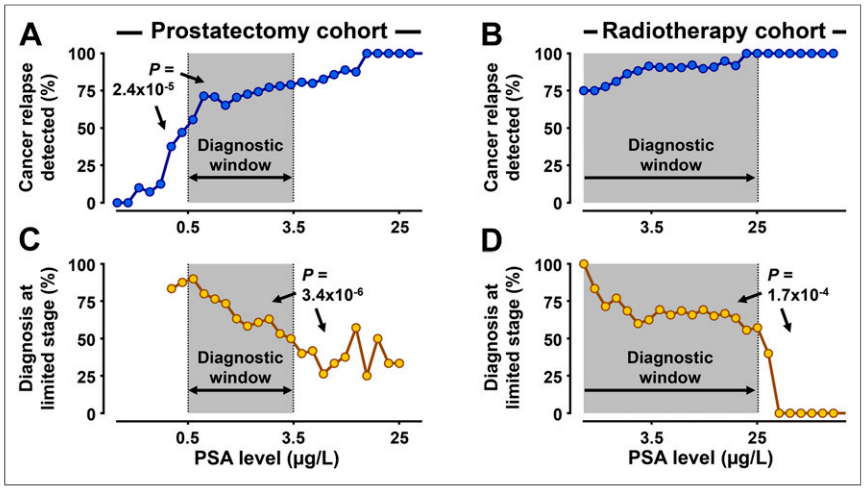

FIGURE 1. PSA-based stratification reveals optimized PSA range for PET imaging. Patients were sorted by log-transformed PSA levels (*x*-axis) in ascending order. Fraction of PSMA-positive scans (blue) is plotted against PSA levels in prostatectomy (A) and radiotherapy (B) patients (PSA sensitivity curve). Similarly, fraction of scans, displaying recurrent tumors at limited stage (gold), is plotted against PSA levels in prostatectomy (C) and radiotherapy (D) patients. On the basis of these curves, diagnostic window (gray) for PSMA PET imaging was derived.

segments tumor-free; partial concordance—all PSMA-positive segments histologically confirmed, but not all PSMA-negative segments tumor-free; false-positive cases—at least 1 PSMA-positive segment lacking histologic confirmation; and full discordance—PSMA-positive segments lacking histologic confirmation, PSMA-negative segments infiltrated by tumor cells.

Statistics and Mathematic Modeling

For PSA stratification, we systematically calculated tracer sensitivity within multiple small PSA ranges. Each PSA interval was characterized in terms of its center and width. On the basis of the detection rate within each interval, we compiled a PSA-stratified tracer sensitivity curve without any a priori assumption of PSA thresholds. Analogously, we derived curves displaying the PSA-stratified rate of diagnosis at limited stage based on multiple small PSA intervals. From these curves, we derived a diagnostic window as follows: the lower threshold was determined as the PSA level, where sensitivity exceeded 50%. The upper threshold was taken as the PSA level, where the fraction of limited relapses detected decreased 50%.

To correct our sensitivity comparison between ^{18}F- and ^{68}Ga-labeled tracers for Gleason scores, we randomly selected matched subcohorts of 30 ^{18}F and 30 ^{68}Ga tracer patients with pairwise equal Gleason scores (1,000 iterations). We then determined the log-transformed ratio between PSA-stratified sensitivity in the ^{18}F subcohort and sensitivity in the ^{68}Ga subcohort for each iteration. We thus obtained log-transformed ratios r_i, with $r_i > 0$, if ^{18}F sensitivity was superior. Finally, we compared r_i against the null hypothesis by a paired *t* test.

RESULTS

PSA Levels Predict Sensitivity of PSMA Imaging After Prostatectomy

We first subdivided the 191 consecutive PET scans into the following groups: PSMA-negative scans ($n = 43$), PSMA-positive scans displaying limited relapse ($n = 85$), and PSMA-positive scans displaying advanced relapse ($n = 63$).

In prostatectomy patients, PSA levels significantly differed between these 3 groups (Supplemental Fig. 1A; supplemental materials are available at http://jnm.snmjournals.org): PSA levels were significantly lower in PET-negative patients than in PET-positive patients displaying limited ($P = 4.3 \times 10^{-3}$) or advanced relapse ($P = 4.9 \times 10^{-7}$). Furthermore, PSA levels differed significantly between limited and advanced-staged relapses ($P = 7.6 \times 10^{-3}$). Interestingly, PSA values did not differ significantly after radiotherapy (Supplemental Fig. 1B). Intriguingly, PSMA accumulated exclusively in locoregional nodes for 75% of prostatectomy patients with limited relapse, which was rarely observed after radiotherapy (17%, $P < 1 \times 10^{-4}$). Most radiotherapy patients with limited relapse displayed tracer accumulation exclusively in the local tumor bed (68%), which was only occasionally detected after prostatectomy (21%, $P < 1 \times 10^{-4}$).

We next plotted PSA levels against the rate of PET-positive patients after prostatectomy. Furthermore, we plotted PSA against the fraction of scans, displaying a relapse at limited stage. Detection rates increased abruptly and significantly ($P = 2.4 \times 10^{-5}$), when PSA concentrations exceeded 0.5 μg/L and remained largely unchanged above this threshold (Fig. 1A). PSA levels tightly anticorrelated with the probability of detecting cancer relapse at limited stage (Fig. 1C): although most relapsed tumors were diagnosed at limited stage for a PSA of less than 3.5 μg/L, this pattern significantly ($P = 3.4 \times 10^{-6}$) reversed when PSA levels exceeded 3.5 μg/L. Interestingly, these rates were largely PSA-independent for PSA levels up to 25 μg/L in the radiotherapy cohort (Figs. 1B and 1D). Although sensitivity was high across all PSA concentrations examined (median, 91.5%), the fraction of limited-stage diagnoses varied stably around a median of 67.5% for PSA up to 25 μg/L.

As an external validation of our imaging results, biopsy and corresponding PET scan were concordant in 86.6% (13/15) of our patients (fully concordant, 73.3%; partially concordant, 13.3%; Supplemental Fig. 2).

^{18}F-DCFPyL Displays Improved Sensitivity in Localization of Relapsed Tumors After Prostatectomy

We plotted PSA-stratified sensitivity curves separately for ^{18}F-DCFPyL and ^{68}Ga-PSMA-HBED-CC and noted that the sensitivity curve of ^{18}F-DCFPyL was discretely, but robustly, shifted toward lower PSA concentrations. For PSA levels around 0.45 μg/L, local sensitivity of ^{18}F-DCFPyL reached 62%, whereas ^{68}Ga-PSMA-HBED-CC detected tumor relapses in 33% of the cases (Supplemental Fig. 3, arrows). The PSA-stratified sensitivity curve of ^{18}F-DCFPyL exceeded the ^{68}Ga-PSMA-HBED-CC curve significantly ($P = 3.4 \times 10^{-3}$) and substantially (average sensitivity, 80% vs. 68%) for a PSA of 0.5–3.5 μg/L.

As an orthogonal approach, we counted the absolute number of PET-positive patients, as detected with either ^{18}F-DCFPyL or ^{68}Ga-PSMA-HBED-CC (Supplemental Table 1). For a PSA of 0.5–3.5 μg/L, we observed significantly ($P = 0.042$, 1-tailed χ^2 test without Yates correction) and substantially (88.2% vs. 65.7%) more relapsed patients with ^{18}F-DCFPyL (15/17) than with ^{68}Ga-PSMA-HBED-CC (23/35). Outside this PSA range, ^{18}F-DCFPyL and ^{68}Ga-PSMA-HBED-CC displayed similar sensitivity (Fig. 2).

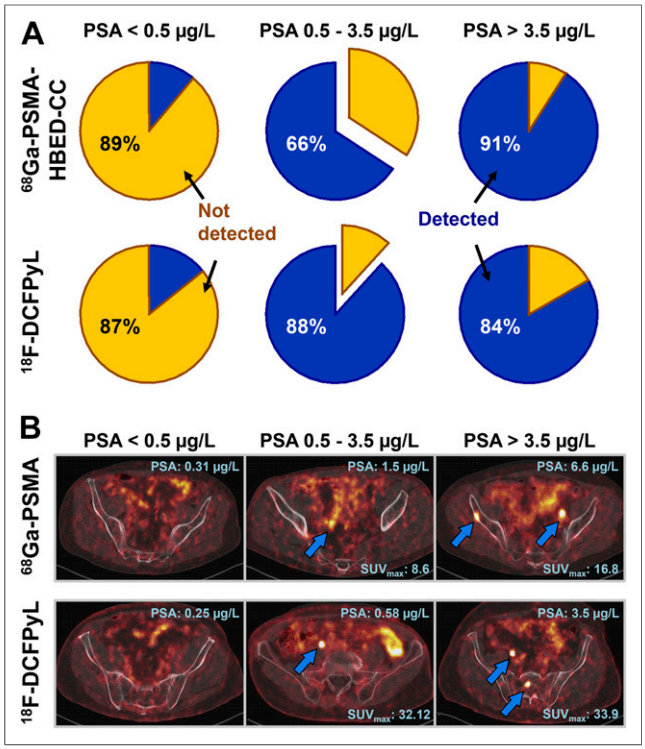

FIGURE 2. ^{18}F-DCFPyL displays enhanced sensitivity for localization of relapsed tumors after prostatectomy at limited stage. (A) Prostatectomy patients with BCR were examined with ^{68}Ga-PSMA-HBED-CC (top) or ^{18}F-DCFPyL (bottom). Pie charts display fractions of PET-positive (blue) and PET-negative (gold) patients with PSA $<$ 0.5 µg/L (left), $>$ 3.5 µg/L (right), or 0.5–3.5 µg/L (middle). (B) Representative PSMA PET/CT images (fusion ratio, 1:1), acquired with ^{68}Ga-PSMA-HBED-CC (top) or ^{18}F-DCFPyL (bottom). PSA level and SUV_{max} over PSMA-positive lesion (blue arrows) are annotated for each scan.

We next aimed to formally exclude the possibility that the substantial sensitivity differences between the 2 tracers might derive from differences in Gleason scores. We performed a mathematic confounder correction and randomly selected 30 Gleason-matched pairs from the ^{18}F and ^{68}Ga tracer cohorts of prostatectomy patients (1,000 iterations) (Supplemental Fig. 4). We then compared PSA-stratified sensitivity of the ^{18}F- and ^{68}Ga-labeled tracers for each iteration. The superiority of ^{18}F-DCFPyL was preserved in 92.1% (all PSA levels, $P = 5.3 \times 10^{-234}$, paired t test against null hypothesis) and 100% (PSA $<$ 1 µg/L, $P = 2.5 \times 10^{-294}$) of the iterations, respectively (Supplemental Figs. 5A and 5B). As a negative control, we randomly swapped tracer labels between matched pairs and found that random relabeling entirely abrogated the significant sensitivity difference between the 2 tracers (Supplemental Figs. 5C and 5D). This suggests that slight differences in Gleason scores cannot sufficiently account for the sensitivity differences between ^{18}F-DCFPyL and ^{68}Ga-PSMA-HBED-CC.

Direct Comparison of Tracer Distribution Patterns in Validation Cohort

We continued our efforts of a recent pilot study (*12*) and sequentially examined patients with ^{68}Ga-PSMA-HBED-CC and ^{18}F-DCFPyL. This gave us a cohort of 25 patients, who had been scanned with both tracers (Fig. 3A). Pairwise comparison of matched PET scans revealed that tracer distribution patterns were highly concordant ($P = 2.71 \times 10^{-8}$), substantiating the validity of ^{18}F-DCFPyL. In particular, all 23 PET-positive lesions on ^{68}Ga scans could be confirmed on the corresponding ^{18}F scan (Fig. 3B).

Intriguingly, for 36% of the ^{68}Ga-PSMA-HBED-CC–positive scans (4/11) we detected additional PET-positive lesions on the ^{18}F-DCFPyL scan (Figs. 3C and 3D). In particular, PET positivity scores were significantly higher for the ^{18}F-DCFPyL scans than for their corresponding ^{68}Ga-PSMA-HBED-CC scans ($P = 4.2 \times 10^{-2}$) (Figs. 3B and 3C). Significance increased when only the matched PET scans of the 11 ^{68}Ga-positive patients were included in the analysis ($P = 3.7 \times 10^{-2}$) (Figs. 3B and 3D).

We next asked whether we could identify any obvious reasons for the increased sensitivity of ^{18}F-DCFPyL. As exemplarily shown in Figure 4, we observed a substantial extinction of tracer signal between the kidneys in ^{68}Ga-PSMA-HBED-CC scans, most likely due to the higher activity of ^{68}Ga-PSMA-HBED-CC in the kidneys, compared with ^{18}F-DCFPyL (*12*). This might explain why this artifact was only marginally present in the corresponding ^{18}F-DCFPyL scan (patient 1). PET-positive lesions could therefore not be reliably excluded between the kidneys on some ^{68}Ga-PSMA-HBED-CC scans. For instance, patient 2 revealed an ^{18}F-DCFPyL–positive metastasis in LVB2, which was largely annihilated in the ^{68}Ga-PSMA-HBED-CC scan (Fig. 4). Additionally, for some patients the visibility of PET-positive lesions was substantially lower with ^{68}Ga-PSMA-HBED-CC than ^{18}F-DCFPyL (patient 3).

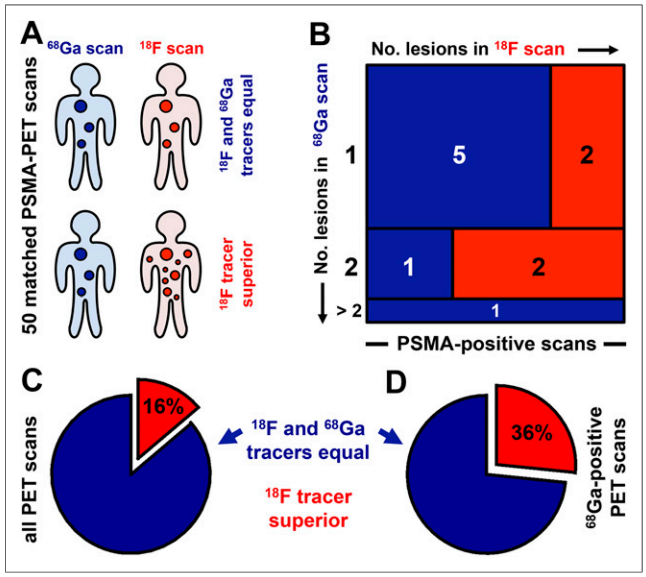

FIGURE 3. Direct comparison of distribution patterns of ^{18}F-DCFPyL and ^{68}Ga-PSMA-HBED-CC. (A) For 25 patients, sequentially examined with ^{18}F-DCFPyL and ^{68}Ga-PSMA-HBED-CC, we determined whether the 2 tracers displayed equal number of lesions. PSMA negativity was consistent for ^{18}F-DCFPyL and ^{68}Ga-PSMA-HBED-CC in all 14 PSMA-negative cases. (B) Mosaic plot compares PET positivity scores between the 2 tracers in all 11 PSMA-positive cases (rows: PET positivity of the ^{68}Ga scan; columns: PET positivity of corresponding ^{18}F scan). Each group is represented by rectangle (red: more ^{18}F-DCFPyL–positive lesions; blue: equal PET positivity scores). Rectangle areas reflect group sizes. (C and D) Pie charts display fraction of patients with superior PET positivity of ^{18}F-DCFPyL scan (red) (all PET scans, 25 patients, C). Alternatively, only patients with positive ^{68}Ga scans were included (^{68}Ga-positive PET scans, 11 patients, D).

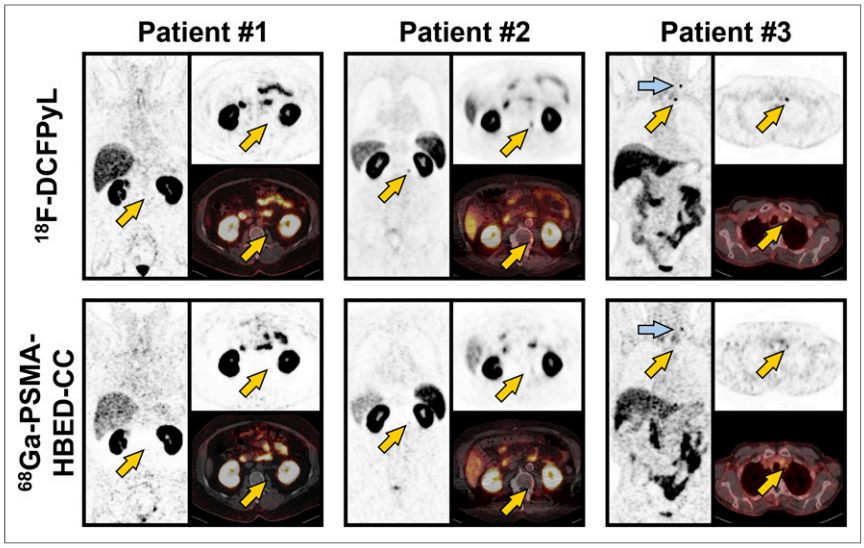

FIGURE 4. Representative matched PET scans. Images are shown for 3 PSMA-positive patients who were examined with ^{18}F-DCFPyL (top) and ^{68}Ga-PSMA-HBED-CC (bottom). Although patients 1 and 2 displayed clear ^{68}Ga signal extinction artifact—that is, low activity counts between kidneys—patient 3 displayed diminished tracer contrast on ^{68}Ga scan. Coronary (left) and transversal (top right) slices are shown for each PET scan. Additionally, PET/CT fusion image is displayed (bottom right). Arrows highlight differences between ^{18}F and ^{68}Ga scans. Same technical parameters (SUV windows, brightness, contrast) were used for each corresponding image pair.

DISCUSSION

PSA Levels Pinpoint Optimized Timing of PSMA PET

Accurate timing of PSMA PET substantially affects its diagnostic value in BCR patients. When PET scans are acquired too early, tumor detection rates are typically low. When PSMA PET scans are acquired too late, the number of patients identified at limited-stage disease is low, thus limiting its value for the individual patient. Our retrospective analyses suggest that the diagnostic value of PET depends on the absolute PSA level of BCR after prostatectomy, in marked contrast to the situation after radiotherapy. We established that a narrow PSA range of 0.5–3.5 μg/L allows optimal detection of cancer relapse after surgery. Thus, narrow monitoring of PSA values could well be useful for accurate timing of PET imaging.

A recent study reported a sensitivity rate of 85% for ^{68}Ga-PSMA-HBED-CC in prostatectomy patients with BCR (*7*), which is fully concordant with our own observations. However, as that study did not subdivide the patient group with a PSA of less than 1 μg/L, lower detection thresholds cannot be derived. Another study reported a detection rate of 58% for patients with a PSA of less than 0.5 μg/L (*5*). A third retrospective study on ^{68}Ga-PSMA-HBED-CC stratified patients using fixed PSA thresholds (*6*); sensitivity was 65% (0.2–0.29 μg/L), 44% (0.3–0.49 μg/L), and 71% (0.5–0.99 μg/L). This wide variability of tracer sensitivity suggests that results may be dependent on the patient cohorts examined, on the PSA thresholds selected, and on interpreter-dependent differences. We therefore compared ^{18}F- and ^{68}Ga-labeled PSMA tracer cohorts that had been simultaneously examined by the same interpreters at the same institution and within the same time period. Furthermore, in contrast to previous studies, we used a mathematic model, which determined tracer sensitivity for variable PSA thresholds. This enabled us to derive a PSA range, optimized for PSMA PET imaging, without a priori definition of PSA thresholds.

Sensitivity of PSMA PET Parallels PSMA Expression

Mannweiler et al. profiled PSMA expression in 51 metastasized prostate cancer patients (*2*). They found that 96% of primary tumors and 84% of the corresponding metastases displayed detectable PSMA levels. We therefore speculated that PSMA PET sensitivity might generally be limited to approximately 84%, due to heterogeneous PSMA expression in prostate cancer (*2*). Concordantly, PET imaging reached a sensitivity rate of 89% in our prostatectomy patients with a PSA of greater than 3.5 μg/L. Furthermore, we found surprisingly high PSA levels of more than 2.5 μg/L in 21% of the PSMA-negative patients, which can most likely be attributed to PSMA-negative metastases. ^{18}F-DCFPyL reached a sensitivity of 88% in prostatectomy patients even for PSA levels of 0.5–3.5 μg/L. We thus speculate that ^{18}F-DCFPyL exploits the full potential of PSMA tracers for a PSA of 0.5 μg/L or more.

^{18}F-DCFPyL Allows Early Localization of Cancer Relapse

On the basis of 62 ^{18}F-DCFPyL scans, this study confirmed previous pilot studies (*11,12*), which reported that ^{18}F-DCFPyL sensitivity is at least noninferior to the ^{68}Ga-PSMA-HBED-CC standard. Intriguingly, in this larger study, ^{18}F-DCFPyL displayed even improved detection rates in prostatectomy patients with PSA levels of 0.5–3.5 μg/L. We used matched-pair analyses to exclude the possibility that Gleason scores might affect differences in tracer sensitivity. Furthermore, we performed cross-sectional imaging of 25 patients with both tracers and found that ^{18}F-DCFPyL detected significantly more PET-positive lesions. As this improved sensitivity of ^{18}F-DCFPyL was thus consistent across 3 independent approaches, our results suggest that it would be well worth validating ^{18}F-labeled PSMA tracers in future prospective trials.

Nevertheless, we note that our study had the following limitations. We derived the lower PSA threshold (0.5 μg/L) retrospectively from our PET imaging results. Below this threshold, our tracer sensitivity rates were substantially lower than the results of previous studies on ^{68}Ga-PSMA-HBED-CC for PSA levels of 0.2–0.5 μg/L (*5,6*). One explanation for this incongruence might lie in our scoring system, whereby a PET-positive lymph node required a morphologic correlate in the corresponding low-dose CT scan. Thus, we cannot formally exclude the possibility that PET-positive lymph nodes without a clear CT-morphologic correlate were misinterpreted as physiologic tracer accumulation in the ureter or intestine. Hence, interobserver variability may affect the lower PSA threshold. Similarly, we defined the upper PSA threshold (3.5 μg/L) based on our PET imaging results. Although none of our PET-negative patients displayed suggestive lesions on the corresponding CT scan, we cannot rule out the possibility that some patients diagnosed as limited stage carried additional PET-negative lesions at distant sites.

The standard tracer acquisition protocols (*3,5,7,12*) used in this study included different tracer uptake time periods for ^{18}F-DCFPyL (120 min) and ^{68}Ga-PSMA-HBED-CC (60 min) before image acquisition, because of the shorter half-life of the ^{68}Ga label. This time difference of 60 min may contribute to the increased sensitivity of

^{18}F-DCFPyL, as a recent pilot study observed that delayed image acquisition improved the quality of ^{68}Ga-PSMA-HBED-CC scans for 4 patients (*8*). Furthermore, standard acquisition protocols (*3,5,7,12*) recommend different activity dosages for ^{18}F-DCFPyL (250 MBq) and ^{68}Ga-PSMA-HBED-CC (150 MBq), because of the small yields of local gallium generators in routine diagnostic procedures. Perhaps not surprisingly, a recent pilot study (*12*) thus reported significantly higher SUV_{max} in tumor lesions for ^{18}F-DCFPyL than ^{68}Ga-PSMA-HBED-CC, which enhances the tumor-to-background ratio of ^{18}F-DCFPyL scans and might thus facilitate their interpretation. Although challenging in routine diagnostics, a potential improvement of the acquisition protocol for ^{68}Ga-PSMA-HBED-CC might thus be prolongation of the acquisition time for PET scans. Our uptake time periods and tracer dosages are in full concordance with standard acquisition protocols of previous studies (*3,5,7,12*). Furthermore, a large prospective trial obtained PET scans with ^{68}Ga-PSMA-HBED-CC after an even shorter time period of 45 min but still observed high sensitivity (*6*). Hence, optimized acquisition protocols for PSMA tracers remain a current matter of debate.

An additional factor, contributing to the increased sensitivity of ^{18}F-DCFPyL, was the reduced tracer signal extinction between the kidneys, which we observed for ^{18}F-DCFPyL. A recent study reported that the quality of ^{68}Ga-PSMA-HBED-CC scans could be improved by delayed imaging after forced diuresis (*9*). In this study, we did not use forced diuresis, although this might well provide a means of improving the performance of both tracers.

Histologic validation was available only for a relatively small subcohort of patients. Hence, tracers could not be compared on the basis of histopathologic results and we cannot formally exclude the possibility that additional ^{18}F-DCFPyL–positive lesions represent false-positive results. Furthermore, we obtained local biopsies exclusively from the prostate fossa of PET-positive patients with limited relapse. Consequently, PET-negative and advanced-staged patients did not undergo biopsy, so that our histopathologic validation was not independent of PET results. However, given the high coincidence between the distribution patterns of ^{68}Ga-PSMA-HBED-CC and ^{18}F-DCFPyL (including subthreshold correlates of ^{18}F-DCFPyL–positive lesions in the corresponding ^{68}Ga-PSMA-HBED-CC scan) as well as the morphologic correlates of PET-positive lesions in the corresponding CT scan, there is accumulating evidence for the validity of ^{18}F-DCFPyL. Four recent studies reported that PSMA-positive lesions could be histologically confirmed in 82%, 94%, 99%, and 100% of cases, respectively (*13–16*).

Despite its limitations, the major strengths of this study are that we provide the largest cohort of BCR patients examined with ^{18}F-DCFPyL to date and that both tracers were used simultaneously at the same institution and analyzed by the same interpreters. Furthermore, we used a wide spectrum of mathematic models, including iterative Gleason-matched-pair analyses, to separately analyze prostatectomy and radiotherapy cohorts. Additionally, we applied variable PSA thresholds without making any a priori assumptions. Finally, we cross-validated our results using a separate cohort of 25 patients who were sequentially examined with both tracers, thus allowing a direct comparison of the distribution patterns of ^{18}F- and ^{68}Ga-labeled PSMA tracers.

CONCLUSION

Our data suggest that ^{18}F-DCFPyL is noninferior to ^{68}Ga-PSMA-HBED-CC while offering all the advantages of ^{18}F labeling. Imaging with ^{18}F-DCFPyL may even exhibit improved sensitivity, when PSA levels are moderately increased to between 0.5 and 3.5 μg/L after prostatectomy. This is of high clinical relevance because within this PSA range PSMA PET imaging detected most relapses at a limited stage. Hence, our findings provide a promising basis for validation of ^{18}F-DCFPyL in future prospective trials.

DISCLOSURE

No potential conflict of interest relevant to this article was reported.

REFERENCES

1. Freedland SJ, Rumble RB, Finelli A, et al. Adjuvant and salvage radiotherapy after prostatectomy: American Society of Clinical Oncology clinical practice guideline endorsement. *J Clin Oncol.* 2014;32:3892–3898.
2. Mannweiler S, Amersdorfer P, Trajanoski S, Terrett JA, King D, Mehes G. Heterogeneity of prostate-specific membrane antigen (PSMA) expression in prostate carcinoma with distant metastasis. *Pathol Oncol Res.* 2009;15:167–172.
3. Afshar-Oromieh A, Avtzi E, Giesel FL, et al. The diagnostic value of PET/CT imaging with the ^{68}Ga-labelled PSMA ligand HBED-CC in the diagnosis of recurrent prostate cancer. *Eur J Nucl Med Mol Imaging.* 2015;42:197–209.
4. Ceci F, Uprimny C, Nilica B, et al. ^{68}Ga-PSMA PET/CT for restaging recurrent prostate cancer: which factors are associated with PET/CT detection rate? *Eur J Nucl Med Mol Imaging.* 2015;42:1284–1294.
5. Eiber M, Maurer T, Souvatzoglou M, et al. Evaluation of hybrid ^{68}Ga-PSMA ligand PET/CT in 248 patients with biochemical recurrence after radical prostatectomy. *J Nucl Med.* 2015;56:668–674.
6. van Leeuwen PJ, Stricker P, Hruby G, et al. ^{68}Ga-PSMA has a high detection rate of prostate cancer recurrence outside the prostatic fossa in patients being considered for salvage radiation treatment. *BJU Int.* 2016;117:732–739.
7. Bluemel C, Krebs M, Polat B, et al. ^{68}Ga-PSMA-PET/CT in patients with biochemical prostate cancer recurrence and negative ^{18}F-choline-PET/CT. *Clin Nucl Med.* 2016;41:515–521.
8. Afshar-Oromieh A, Hetzheim H, Kubler W, et al. Radiation dosimetry of ^{68}Ga-PSMA-11 (HBED-CC) and preliminary evaluation of optimal imaging timing. *Eur J Nucl Med Mol Imaging.* 2016;43:1611–1620.
9. Derlin T, Weiberg D, von Klot C, et al. ^{68}Ga-PSMA I&T PET/CT for assessment of prostate cancer: evaluation of image quality after forced diuresis and delayed imaging. *Eur Radiol.* 2016;26:4345–4353.
10. Chen Y, Pullambhatla M, Foss CA, et al. 2-(3-{1-carboxy-5-[(6-[^{18}F]fluoro-pyridine-3-carbonyl)-amino]-pentyl}-ureido)-pen tanedioic acid, [^{18}F]DCFPyL, a PSMA-based PET imaging agent for prostate cancer. *Clin Cancer Res.* 2011;17:7645–7653.
11. Szabo Z, Mena E, Rowe SP, et al. Initial evaluation of [^{18}F]DCFPyL for prostate-specific membrane antigen (PSMA)-targeted PET imaging of prostate cancer. *Mol Imaging Biol.* 2015;17:565–574.
12. Dietlein M, Kobe C, Kuhnert G, et al. Comparison of [^{18}F]DCFPyL and [^{68}Ga] Ga-PSMA-HBED-CC for PSMA-PET imaging in patients with relapsed prostate cancer. *Mol Imaging Biol.* 2015;17:575–584.
13. Budäus L, Leyh-Bannurah SR, Salomon G, et al. Initial experience of ^{68}Ga-PSMA PET/CT imaging in high-risk prostate cancer patients prior to radical prostatectomy. *Eur Urol.* 2016;69:393–396.
14. Eiber M, Weirich G, Holzapfel K, et al. Simultaneous Ga-PSMA HBED-CC PET/MRI improves the localization of primary prostate cancer. *Eur Urol.* 2016;70:829–836.
15. Maurer T, Gschwend JE, Rauscher I, et al. Diagnostic efficacy of gallium-PSMA positron emission tomography compared to conventional imaging for lymph node staging of 130 consecutive patients with intermediate to high risk prostate cancer. *J Urol.* 2016;195:1436–1443.
16. Herlemann A, Wenter V, Kretschmer A, et al. Ga-PSMA positron emission tomography/computed tomography provides accurate staging of lymph node regions prior to lymph node dissection in patients with prostate cancer. *Eur Urol.* 2016;70:553–557.
17. Roesch F. Maturation of a key resource: the germanium-68/gallium-68 generator: development and new insights. *Curr Radiopharm.* 2012;5:202–211.
18. Alva-Sánchez H, Quintana-Bautista C, Martinez-Davalos A, Avila-Rodriguez MA, Rodriguez-Villafuerte M. Positron range in tissue-equivalent materials: experimental microPET studies. *Phys Med Biol.* 2016;61:6307–6321.
19. Eder M, Schäfer M, Bauder-Wust U, et al. ^{68}Ga-complex lipophilicity and the targeting property of a urea-based PSMA inhibitor for PET imaging. *Bioconjug Chem.* 2012;23:688–697.
20. Schäfer M, Bauder-Wust U, Leotta K, et al. A dimerized urea-based inhibitor of the prostate-specific membrane antigen for ^{68}Ga-PET imaging of prostate cancer. *EJNMMI Res.* 2012;2:23.
21. Armstrong IS, Kelly MD, Williams HA, Matthews JC. Impact of point spread function modelling and time of flight on FDG uptake measurements in lung lesions using alternative filtering strategies. *EJNMMI Phys.* 2014;1:99.